Analyst

Accepted Manuscript

ROYAL SOCIETY OF CHEMISTRY

www.rsc.org/analyst

Fine Structural Features of Nanoscale Zero-Valent Iron Characterized by Spherical Aberration Corrected Scanning Transmission Electron Microscopy (Cs-STEM)

Airong Liu and Wei-xian Zhang[1]
State Key Laboratory for Pollution Control and Resource Reuse
School of Environmental Science and Engineering
Tongji University
Shanghai, China 200092

Abstract

An angstrom-resolution physical model of nanoscale zero-valent iron (nZVI) is generated with a combination of spherical aberration corrected scanning transmission electron microscopy (**Cs**-STEM), selected area electron diffraction (SAED), energy-dispersive X-ray spectroscopy (EDS) and electron energy-loss spectroscopy (EELS) on the Fe *L*-edge. Bright-field (BF), high-angle annular dark-field (HAADF) and secondary electron (SE) imaging of nZVI acquired by a Hitachi HD-2700 STEM present near atomic resolution images and detailed morphological and structural information of nZVI. The STEM-EDS technique confirms that the fresh nZVI comprises of a metallic iron core encapsulated with a thin layer of iron oxides or oxyhydroxides. SAED patterns of the Fe core suggest the polycrystalline structure in the metallic core and amorphous nature of the oxide layer. Furthermore, Fe *L*-edge of EELS shows varied structural features from the innermost Fe core to the outer oxide shell. Particularly, a qualitative analysis of the Fe $L_{2,3}$ edge fine structures reveals that the shell of nZVI consists of a mixed Fe (II)/Fe (III) phase close to the Fe (0) interface and a predominantly Fe (III) at the outer surface of nZVI.

[1] To whom all correspondence should be addressed. Tel: +86-21-6598-2684; Fax: +86-21-6598-3689
E-mail address: zhangwx@tongji.edu.cn (Wei-xian Zhang)

1 Introduction

Nanoscale zero-valent iron (nZVI) is a multifunctional nanomaterial for treatment of a growing number of toxic and hazardous substances, including both organic (e.g., halogenated hydrocarbons)[1-5] and inorganic (e.g., nitrate, chromate, perchlorate, metal ions) contaminants in the environment.[6-11] Favorable chemical and physical factors of nZVI contribute to its increasing environmental applications. nZVI has a core-shell structure with a metallic core surrounded by an iron oxide/hydroxide shell.[12-17] The core-shell structure with two nano-constituents bestows multifaceted chemical properties for contaminant removal and transformation: the metallic iron serves as an electron source and exerts a reducing character, while the oxide shell facilitates sorption of contaminants via electrostatic interactions and surface complexation, and at the same time, permits efficient electron passage from the metal core to the surface. The defective and disordered nature of the oxide shell renders it potentially more reactive than a plain passive oxide layer on top of bulk iron materials.[17] Current understandings on the structure of nZVI are based on a combination of spectroscopic and diffractometric methods whose spatial resolution is larger than the key features of core-shell nanoparticles.[14-19]

For study of chemical reactions in solid materials, STEM provides enhanced capability on direct physical imaging and chemical identification at atomic resolution.[20-23] The spherical aberration corrector allows a larger probe current to be focused in a very fine probe, making atomic resolution spectroscopy possible. Bright field (BF) STEM imaging mode allows structure

imaging on the basis of phase contrast similar to a typical transmission electron microscopy imaging. High-angle annular dark-field (HAADF) STEM imaging, which uses high-angle elastic (or phonon) scattering, enables high-spatial-resolution (0.14 nm) imaging. By integrating energy-dispersive X-ray spectroscopy (EDS) with the Cs-STEM techniques,[24-26] direct visualization of nanoscale structural and compositional evolution at atomic scale can be achieved at the same time. Furthermore, elemental and chemical bonding information can be obtained from electron energy-loss spectroscopy (EELS) on both O *K*-edge and Fe *L*-edge. For example, EELS can probe atom bonding environments, and thus **provides** valuable information regarding the elemental valences of the particle.

Objective of work is to obtain STEM imaging with detailed physical and chemical information of nZVI at atomic resolution. The state-of-the-art Cs-STEM is applied to obtain direct evidence on the core-shell structure of nZVI and elemental distributions of nZVI. High spatial resolution images are then applied to construct a high-resolution model of fresh nZVI and interpret chemical reaction mechanisms in nZVI.

2 Experimental Section

2.1 Preparation of Nanoscale Zero-Valent Iron

Procedures used in the preparation of iron nanoparticles have been published previously.[27,28] The procedures are based on chemical reduction and precipitation of ferric ion with sodium borohydride in water. The

nanoparticle aggregates are collected by vacuum filtration and refrigerated in a sealed polyethylene container at 4°C under 95% ethanol until use. The residual water content of the nanoparticles as used typically varies between 40 and 50%. Average size of the synthesized nZVI is 60 nm with BET surface approximately at 30 m^2/g.

2.2 Electron Microscopy Analysis

Samples for the STEM analysis is prepared by allowing a drop of a dilute ethanol suspension of the nanoparticles to dry on a lacey-carbon film supported on a 300-mesh copper STEM grid. A Hitachi HD-2700 STEM operated at 200 kV is used. A schematic of Hitachi HD-2700 STEM is provided in supporting information (Fig. S1). The Hitachi HD-2700 allows simultaneous acquisition of bright-field (BF), high-angle annular dark-field (HAADF), secondary electron (SE) imaging, as well as electron diffraction.

3 Results and Discussion

3.1 Structural Features Derived from STEM Imaging

3.1.1 STEM Imaging

Low magnification STEM images (Fig. 1a, b, c at 50,000X) show morphology and degree of nZVI aggregation through SE, BF and HADDF imaging. The nanoparticles are mostly spherical in shape with majority in the size range of 50-100 nm and present as chain-like aggregates. The connected

nanoparticles have a continuous oxide shell, but the metallic cores are separated from each other by a thin (~1 nm) interfacial iron oxide layer.

The SE images (Fig.1a, d, g) offer near three-dimensional characteristics of the nZVI particles. The images constructed from secondary electron diffraction clearly give rich depth information about the particle surface. Figure 1b, e, h show a series of HAADF images of nZVI. HAADF images are often described as the Z-contrast (atomic number) imaging since the measured intensity is approximately proportional to the square of the atomic number. **The STEM-HAADF imaging mode** is a high-resolution technique that generates readily interpretable images of nanoscale structures,[29] that is, regions of the specimen with greater atomic number appear brighter in the image. For example, the particles in Figure1 b, e, h consist of a bright core, corresponding to the metallic iron. The outer layer composed of oxygen and iron is darker than the core area.

According to the BF images (Fig.1c, f, i), the surface layer has a thickness of 2-3 nm and is more transparent than the core region. The BF imaging mode, complementary to HAADF allows observations of inherent structures on the basis of phase contrast similar to typical TEM imaging. It is clearly shown in the image (Fig. 1i, at 900,000 multiples) that a single particle comprises of a dense core surrounded by a thin shell exhibiting markedly less contrast than the core area.

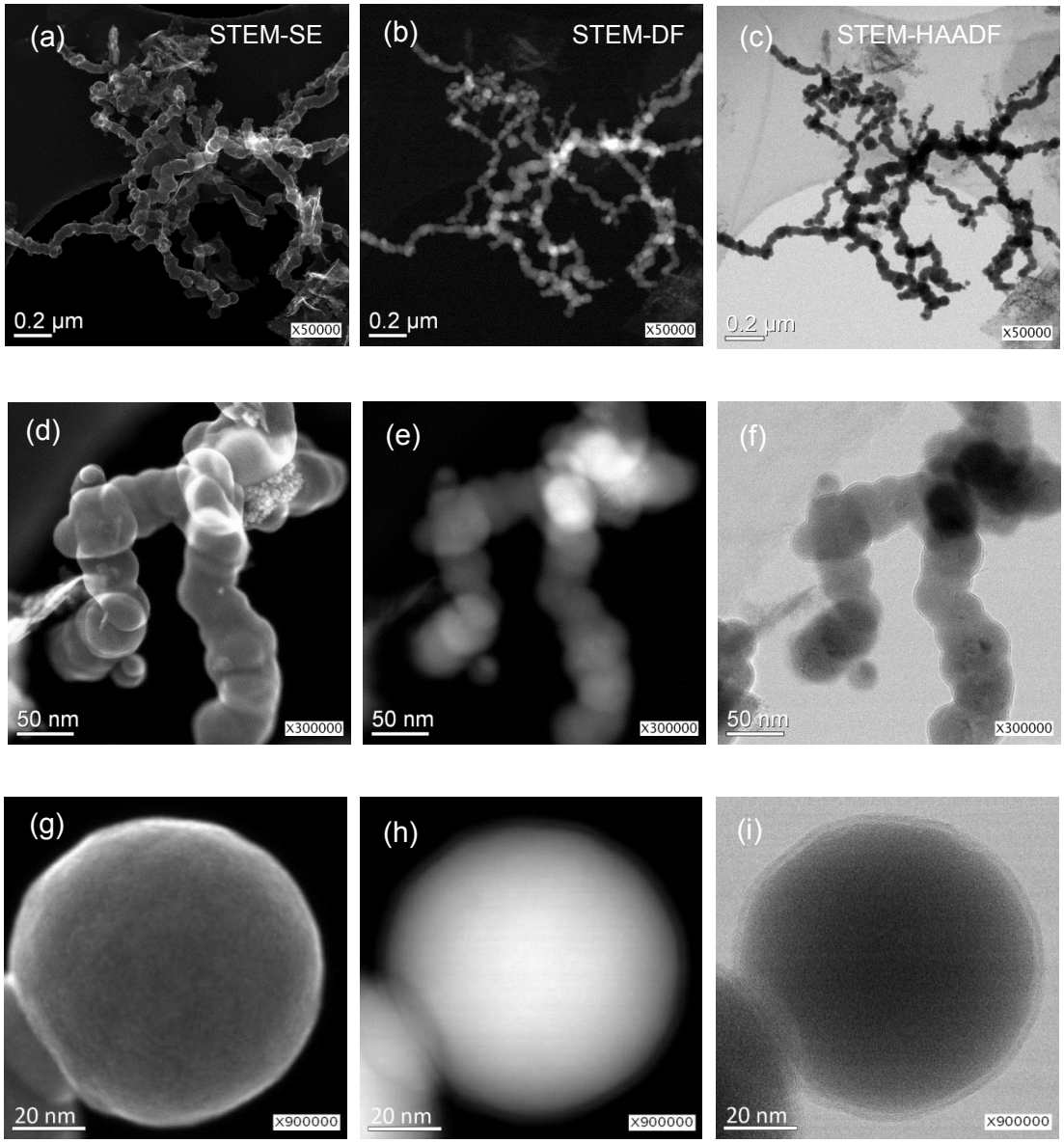

Fig. 1. STEM images of fresh nZVI at different magnifications (50,000, 300,000, 900,000 multiples): a, d, g are secondary electrons (SE) images; b, e, h are HAADF images using transmitted electrons and c, f, i are bright field (BF) images. All images were acquired with a Hitachi HD-2700 STEM

3.1.2 High resolution STEM and corresponding SAED analysis of nZVI core

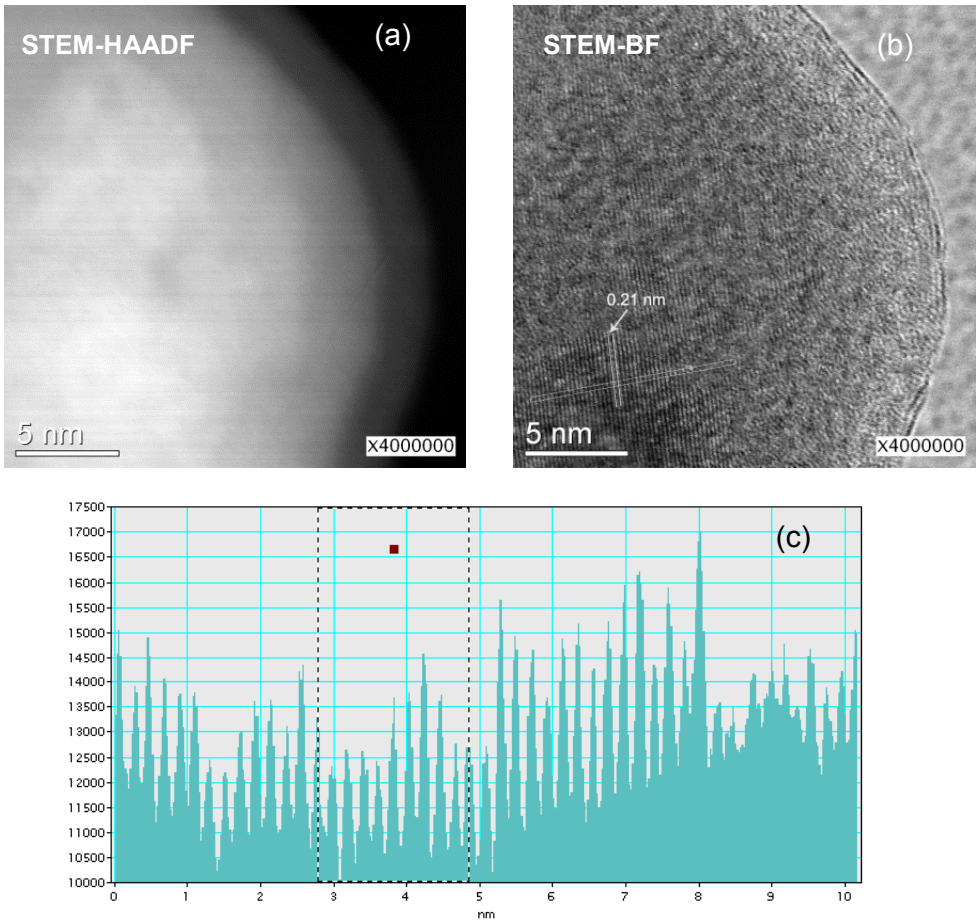

Fig. 2 High resolution STEM images of fresh nZVI: (a) STEM-HAADF; (b) STEM-BF; (c) intensity profile of the designated area in (b), showing the lattice fringe at 0.21 nm.

To gain further insights on the fine structures of nZVI, high-resolution STEM analysis is performed. Representative results are given in Figure 2, which includes high-resolution HAADF and BF micrographs. The HAADF image (Fig. 2a) shows clear contrast changes from the outer layer to inner sphere of a nano particle. HAADF imaging of nZVI has high compositional sensitivity compared with conventional transmission electron microscopy and

enables higher spatial resolution images. The larger contrast corresponds to the high density of iron materials, whereas the lighter contrast suggests a mixture of lighter elements (e.g., O).

The BF imaging (Fig. 1b) clearly shows that the metallic core has typical long-range regular structures and the oxide shell on the other hand is amorphous, which was previously assigned as FeOOH. [4, 27] The disordered oxide layer can be partly explained by the extremely small radii of the nanoparticle and the curvature of the oxide shell, which imposes considerable strains hindering the crystalline formation. Moreover, the presence of a small amount of boron in the oxide film from borohydride precursor used in the synthesis may contribute to defective sites and alter the oxide structure as shown in Figure 2b.[18, 27] The lattice fringe spacing is measured at 0.21 nm (Fig. 2c) within the typical range of the interplanar spacing of α-Fe (110).[30]

As shown in Figure 2c, the intensity profile of the designated area further supports the results shown in Figure 2b. As previously reported, results are also in good agreement with the XRD pattern. In short, the core of nZVI is most likely α-Fe (110).[30]

3.1.3 SAED analysis of the shell layer

Figure 3a-d shows a STEM-BF image and electron diffractions of the three selected areas in a nZVI nanoparticle. Point 1 is close to the metallic core. SAED analysis of point 1 (**Fig. 3b**) shows the presence of diffuse rings, suggesting that the particle core is polycrystalline. All the diffraction rings in the SAED pattern can be indexed as α-Fe phase (JCPDS 65-4899) with (110),

(200), (211) plane from the insider to the surface.[30] The scattered rings of SAED pattern of Point 1 shows that the area in this particle is not perfect crystalline, due to the closeness to the external interface of metallic core.

Point 2 is located at the interface of metallic iron and iron oxides, and Point 3 within the oxide shell. SAED patterns of the two areas show the irregular atomic arrangements. The SAED pattern of Point 3 is more irregular than that of Point 2, which is also consistent with previous studies. [8,15,19] There is a notable absence of a lattice fringe and perfect diffuse rings in SAED pattern, indicating that the particles are poorly ordered and amorphous; similar results were further confirmed by the broad peaks in XRD analysis.

The microscopic structure of the oxide shell is inherently different from bulk iron oxides with shell of nZVI less ordered in structure. The defective nature of the oxide phase offers enhanced electron-transfer and mass transport capabilities. The exact arrangements of the oxide structure also depend on the synthesis process, particle size and storage conditions. [30]

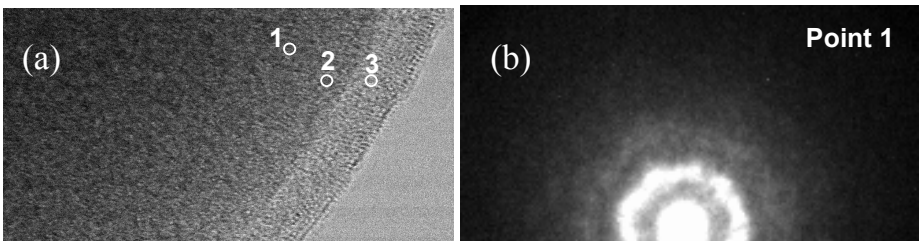

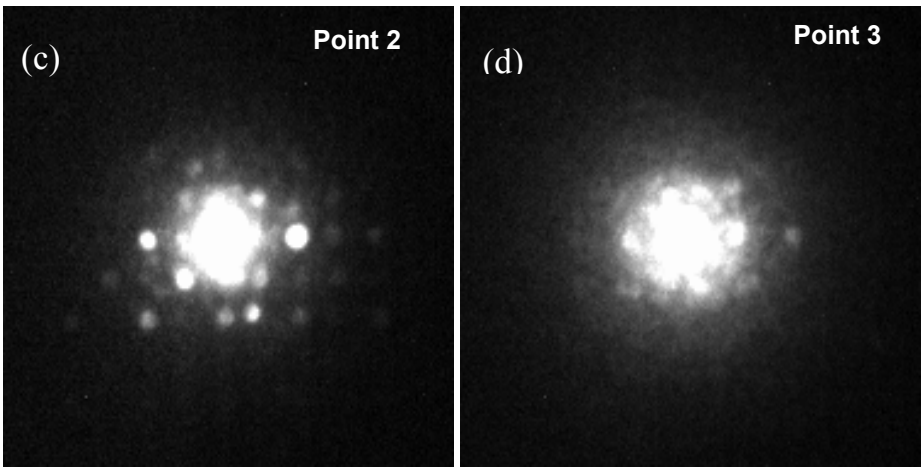

Fig. 3 High magnification STEM-BF image (3,500,000X) (a), in which three points are selected for SAED analysis. Point 1 is in the outer core area (b), Point 2 is near the core-shell interface(c), and Point 3 is within the oxide layer (d).

3.2 EDS Analysis

Elemental distributions of Fe and O in a nZVI particle are characterized using the STEM-EDS method (Fig. 4). Adding a Cs corrector allows a large probe current to be focused on a very fine electron probe, and enables EDS to map elements at sub-nanometer scale resolution (<0.14 nm for the Hitachi HD-2700).

3.2.1 EDS Elemental Mapping

Figure 4 presents a HAADF image (**Fig. 4a**) and the corresponding EDS elemental maps (Fig.4b-d) of a typical nZVI nanoparticle. Elements of Fe, O are denoted in blue and red respectively in the figure. As shown in Figure 4b, the Fe K_α signal exhibits strong intensity in the particle center and a sharp decline in the shell layer. In contrast, the presence of O atoms is mainly within the surface layer. From the O mapping, a ring of 2-4 nm is apparent, which is in agreement with the shell thickness. [13] Overlay of the two elemental maps is shown in Figure 4d, which clearly illustrates the spatial presence of the amorphous oxide phase both at the particle surface and in space between the two particles. The STEM-EDS technique employed in this study is able to map out elemental distribution at a nanometer-scale spatial resolution, and provides a detailed physical model of the layered structure in nZVI. While the nZVI structure has been characterized by various microscopic, spectroscopic and chemical reduction methods in recent studies,[13,15,27] direct visual presentation of the chemical composition and the micro-structure at such a high resolution has yet been reported.

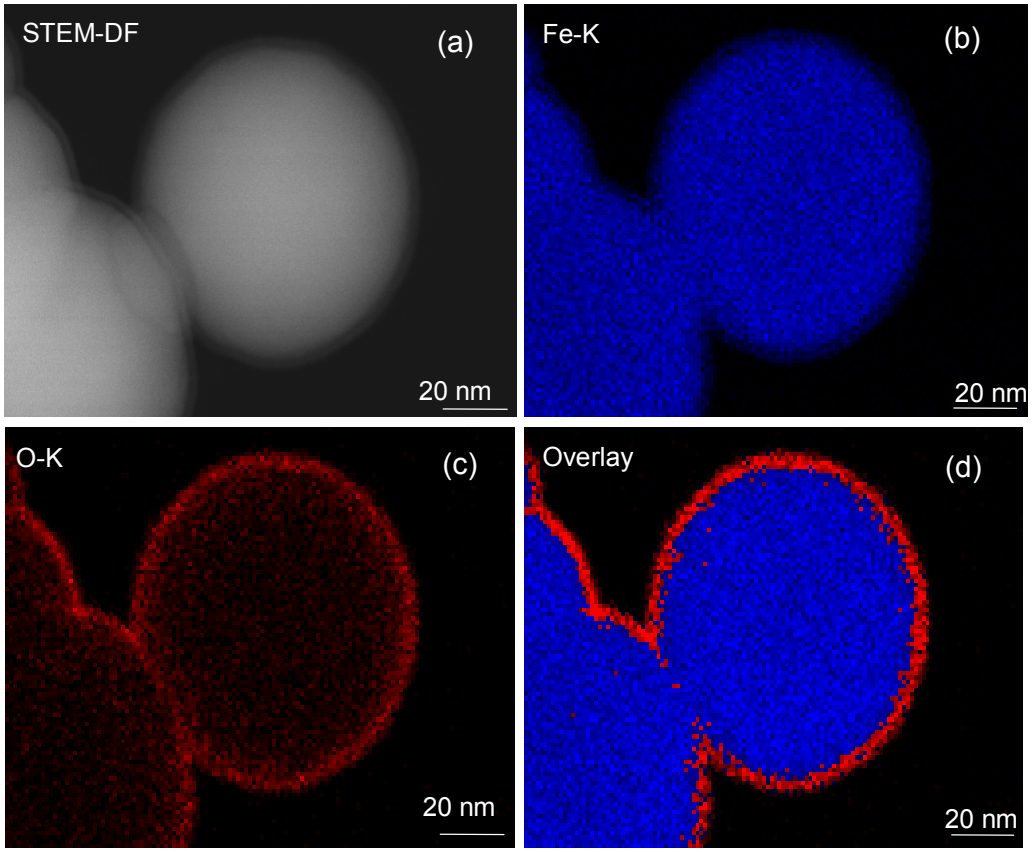

Fig. 4 STEM-HAADF image (a) and STEM-EDS elemental mappings of the Fe K_{α} (b) and O K_{α} (c), X-ray signals collected from fresh nZVI particles. (d) is an overlay of Fe and O.

3.2.2 EDS Line Scan

High-resolution STEM further enhances the capability of EDS. The scanning of elemental distributions can be done on a very small particle in a given direction or area of the particles, and more importantly at angstrom resolution. In this work, the EDS line scan is applied to measure the relative concentrations of iron, oxygen across the iron oxide shell and also over a whole particle.

Figure 5 shows the EDS line profiles of oxygen and iron. The white straight line crossing the interface region in the STEM-HAADF image (Fig. 5a) shows the trajectory of the EDS line scan. On the oxygen line profile (**Fig. 5b**), one main peak accompanied by two shoulder peaks can be clearly identified with the O peak at the interface between the metallic core and oxide shell. In other words, the highest concentration of oxygen exists right at the interface. It can be further deduced that the component in the inner layer of the oxide shell was mainly ferrous hydroxide ($Fe(OH)_2$). The outer surface was composed of multiple components, such as wüstite (FeO), magnetite (Fe_3O_4), maghemite (γ-Fe_2O_3), ~~**(hematite (α-Fe_2O_3),)**~~ and FeOOH , etc.[7,30] In aquatic media, the surface of the oxide is covered with hydroxide groups, giving rise to an apparent stoichiometry close to FeOOH. [13] According to the chemical formula, the O/Fe ratio in the inner layer is about 2, the main component in the inner layer is approximately ferrous hydroxide ($Fe(OH)_2$). At the outer surface due to the presence of multi-components, the ratio of O/Fe is less than 2. In summary, the composition in the iron oxide shell determines the location of the oxygen peaks in the profile. The EDS counts of iron in Fe-line profile increase with the depth into the particle, and gradually reach to a steady plateau, which supports the model of the core-shell structure.[12,13]

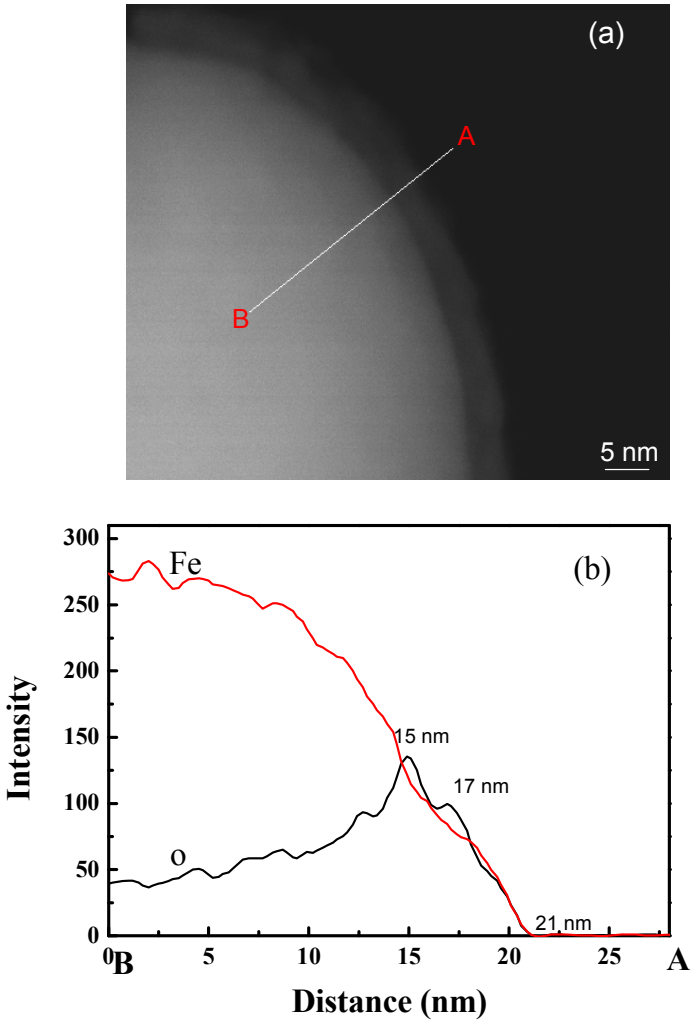

Fig. 5 EDS line profiles of fresh nZVI. (a) STEM-DF image showing line profile trajectory; (b) line profiles of O, Fe.

3.3 Core-Shell Structure Analysis with EELS

Core-level EELS spectroscopy can provide local electronic information at the sub-nanometer spatial resolution. For instance, fine structure EELS investigations of nanoscale systems involving transition-metal 2p→3d excitations can yield valence state quantification, also information on charge transfer and crystal field modification at the atomic scale.[31] The EELS fine

structures of both the O *K*-edge and the Fe $L_{2.3}$-edges imprint these structural differences and therefore can be used to identify a specific Fe phase.[19] The valence state of Fe can often be determined from the following three aspects of the Fe $L_{2.3}$ EELS fine structure spectrum: chemical shift (dependence of the edge position with respect to the valence), fine structural features (splitting of the peaks), and the white-line ratios of the Fe L_2 and Fe L_3 spectra. In particular, spatially resolved EELS analysis on the Fe $L_{2,3}$ edge fine structures can determine iron(II) and iron(III), and yields a much more precise description of the core-shell structure. [10, 30, 32-35]

The HAADF image in **Figure 6a** shows a quarter of one nanoparticle and locations where the five EELS spectra are acquired. The EELS scans progress from the solution-nZVI interface to the core area. The five spectra in the energy loss region of Fe $L_{2,3}$ edges appear in **Figure 6b**. The L_3 peak is situated at 708.8 eV in the spectrum acquired at the surface (point 1), 708.6 eV in the middle of the oxide layer (point 2), 708.4 eV in the oxide-ZVI interface (point 3) and 708.2 eV recorded in the core area (points 4 and 5). The L_2 peaks are located at 723.2 eV (point 1), 721.4 eV (point 2), and 721.2 eV (points 4 and 5) respectively.

The chemical shift on the positions of the L_3 and L_2 peaks from the surface to the core area is apparent. This change of chemical shift in the fine structure of the spectra correlates with changes in the oxidation state of iron. According to Gálvez et al., the much bigger L_3 value of chemical shift shows a maximum

for iron (III) species.[35-36] Consequently, the EELS results in this paper represent clearly evidence on the presence of a higher fraction of iron (III) species at the surface. These results are in agreement with findings of previous XPS studies that the shell of nZVI consisted of a mixed Fe (II)/Fe (III) phase close to the Fe (0) interface and a predominantly Fe (III) oxide at the exterior surface of the nanoparticles.[37-38]

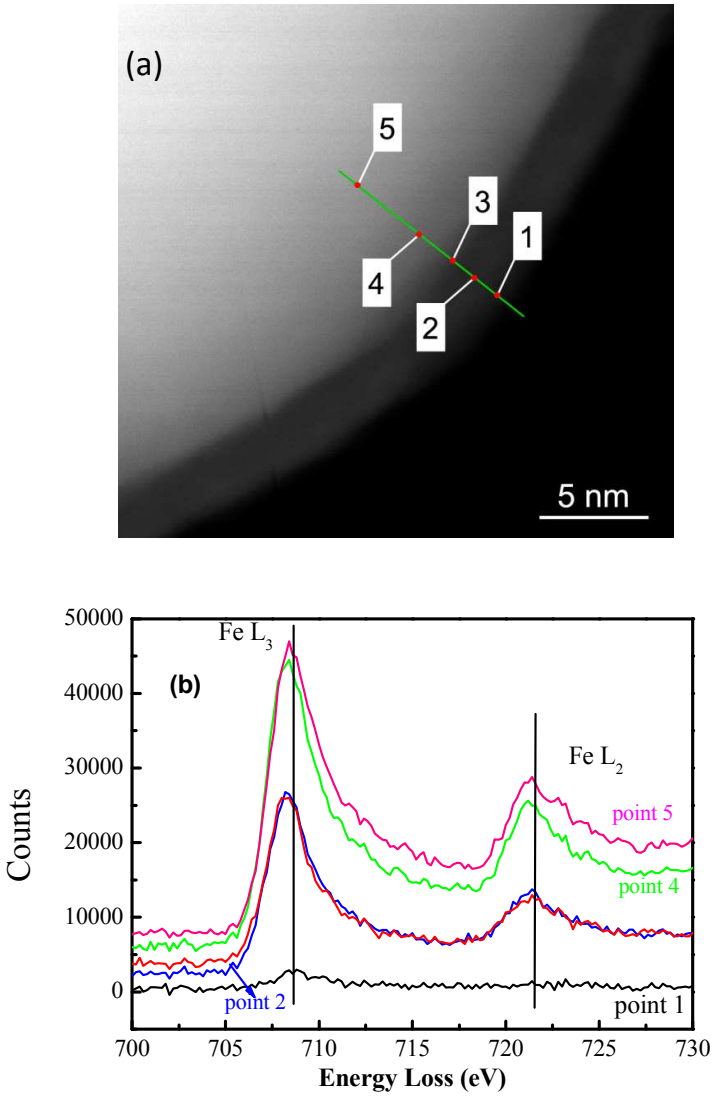

Fig.6 EELS spectra of nZVI recorded across the shell layer. (a) Five points marked in the annular dark-field indicate locations of EELS scan. (b) The iron L-edges of the five positions on the green line.

4 Conclusions

Detailed structural characterization is essential to the understanding on the environmental reactivity and functions of nZVI. In this work, a sub-angstrom resolution physical model of nZVI is obtained with a combination of STEM, SAED, EDX, and EELS on the Fe *L*-edge. Images of nZVI acquired

by a Hitachi HD-2700 STEM provide detailed morphology and structure information. **Cs-corrected** STEM-EDS technique illustrates that the nZVI nanoparticle comprises of a metal iron core encapsulated by a thin layer of iron oxides or oxyhydroxides. Patterns of SAED suggest polycrystalline structures in the core area and confirm the amorphous structures of the surface layer. The unique configuration and the nature of the core-shell structure allow the particle to possess the reductive character of metallic iron and the adsorptive and coordinative properties of iron oxides. The Fe *L*-edge of EELS shows varied chemical features from the innermost Fe core to the outermost oxide shell. It demonstrates that the shell of nZVI consists of a mixed Fe (II)/Fe (III) phase close to the Fe (0) interface and a predominantly Fe (III) oxide at the exterior surface of the nanoparticle. The defective nature of the oxide shell is expected to influence the chemical activity and lifetime in the aqueous environment.

Acknowledgments

Research described in this work has been supported by the Science and Technology Commission of Shanghai (Grant 11JC1412600) and by the National Science Foundation of China (NSFC Grants 21277102, 21003151). The authors thank Hitachi High-Technologies Corporation for the use of HD-2700 STEM and Dr. Xiaofeng Zhang for his assistance in the STEM analysis and interpretation.

Reference

1. C. B. Wang and W. X. Zhang, Synthesizing nanoscale iron particles for rapid and complete dechlorination of TCE and PCBs, *Environ. Sci. Technol.*, 1997**, 31**, 2154–2156.
2. D. W. Elliott and W. X. Zhang, Field assessment of nanoscale bimetallic particles for groundwater treatment, *Environ. Sci. Technol.*, 2001**, 35**, 4922–4926.
3. G. V. Lowry and K. M. Johnson, Congener-specific dechlorination of dissolved PCBs by microscale and nanoscale zerovalent iron in a water/methanol solution, *Environ. Sci. Technol.,* 2004, **38**, 5208–5216.
4. X. Q. Li, D.W. Elliott and W. X. Zhang, Zero-valent iron nanoparticles for abatement of environmental pollutants: materials and engineering aspects, *Crit. Rev. Solid State*., 2006, **31**, 111–122.
5. Y. H. Tee, E. Grulke and D. Bhattacharyya, Role of Ni/Fe nanoparticle composition on the degradation of trichloroethylene from water, *Ind. Eng. Chem. Res.,* 2005, **44**, 7062–7070.
6. S. M. Ponder, J. G. Darab and T. E. Mallouk, Remediation of Cr (VI) and Pb (II) aqueous solutions using supported, nanoscale zero-valent iron, *Environ. Sci. Technol.*, 2000, **34**, 2564–2569.
7. S. R. Kanel, B. Manning, L. Charlet and H. Choi, Removal of arsenic(III) from groundwater by nanoscale zero-valent iron, *Environ. Sci. Technol.*, 2005, **39**, 1291–1298.
8. X. Q. Li and W. X. Zhang, Sequestration of metal cations with zerovalent iron nanoparticles — A study with high resolution X–ray photoelectron spectroscopy (HR–XPS), *J. Phys. Chem. C*, 2007, **111**, 6939–6946.
9. J. Antony, Y. Qiang, D. R. Baer and C. M. Wang, Synthesis and characterization of stable iron–iron oxide core–shell nanoclusters for environmental applications, *J. Nanosci. Nanotechnol.,* 2006, **6,** 568–572.
10. S. M. Ponder, J. G. Darab, J. Bucher, D. Caulder, I. Craig, L. Davis, N.

Edelstein, W. Lukens, H. Nitsche, L. F. Rao, D. K. Shuh and T. E. Mallouk, Surfacechemistry and electrochemistry of supported zerovalent iron nanoparticles in the remediation of aqueous metal contaminants, *Chem. Mater.*, 2001, **13**, 479–486.

11. S. R. Kanel, B. Manning, L. Charlet and H. Choi, Arsenic (V) Removal from Groundwater Using Nano Scale Zero-Valent Iron as a Colloidal Reactive Barrier Material, *Environ. Sci. Technol.*, 2006, **40**, 2045-2050.
12. T. Masciangioli and W. X. Zhang, Environmental technologies at the nanoscale, *Environ. Sci. Technol.,* 2003, **37**, 102A-108A.
13. J. E. Martin, A. A. Herzing, W. L. Yan, X. Q. Li, B. E. Koel, C. J. Kiely and W. X. Zhang, Determination of the Oxide Layer Thickness in Core–Shell Zerovalent Iron Nanoparticles, *Langmuir*, 2008, **24**, 4329–4334.
14. M. A. V. Ramos, W. Yan, X. Q. Li, B. E. Koel and W. X. Zhang, Simultaneous Oxidation and Reduction of Arsenic by Zero-Valent Iron Nanoparticles: Understanding the Significance of the Core-Shell Structure, *J. Phys. Chem. C,* 2009, **113**, 14591-14594.
15. J. T. Nurmi, P. G. Tratnyek, V. Sarathy, D. R. Baer, J. E. Amonette, K. Pecher, C. M. Wang, J. C. Linehan, D. W. Matson, R. L. Penn and M. D. Driessen, Characterization and properties of metallic iron nanoparticles: Spectroscopy, electrochemistry, and kinetics, *Environ. Sci. Technol.*, 2005, **39**, 1221–1230.
16. C. M. Wang, D. R. Baer, J. E. Amonette, M. H. Engelhard, Y. Qiang and J. Antony, Morphology and oxide shell structure of iron nanoparticles grown by sputter–gas–aggregation, *Nanotechnol.,* 2007, **18**, 255603.
17. L. Signorini, L. Pasquini, L. Savini, R. Carboni, F. Boscherini, E. Bonetti, A. Giglia, M. Pedio, N. Mahne and S. Nannarone, Size–dependent oxidation in iron/iron oxide core–shell nanoparticles, *Phys. Rev. B.*, 2003, **68**, 195423.
18. E. E. Carpenter, S. Calvin, R. M. Stroud and V. G. Harris, Passivated iron

as core-shell nanoparticles, *Chem. Mater.*, 2003, **15**, 3245-3246.

19. C. M. Wang, D. R. Baer, J. E. Amonette, M. H. Engelhard, J. Antony and Y. Qiang, Morphology and Electronic Structure of the Oxide Shell on the Surface of Iron Nanoparticles, *J. Am. Chem. Soc.,* 2009, **131**, 8824-8832.
20. **K. Kimoto, T. Asaka, T. Nagai, M. Saito, Y. Matsuil and K. Ishizuka**, Element–selective imaging of atomic columns in a crystal using STEM and EELS, *Nature,* 2007, **450**, 702–704.
21. D. A. Muller, Structure and bonding at the atomic scale by scanning transmission electron microscopy, *Nature Mater.*, 2009, **8**, 263–270.
22. N. D. Browning, M. F. Chisholm and S. J. Pennycook, Atomic-resolution chemical analysis using a scanning transmission electron microscope, *Nature*, 1993, **366**, 143-146.
23. D. A. Muller, L. Fitting Kourkoutis, M. Murfitt, J. H. Song, H. Y. Hwang, J. Silcox, N. Dellby and O. L. Krivane, Atomic-Scale Chemical Imaging of Composition and Bonding by aberration-Corrected Microscopy, *Science,* 2008, **319**, 1073-1076.
24. S. J. Pennycook and L. A. Boatner, Chemically sensitive structure–imaging with a scanning transmission electron microscope, *Nature,* 1988, **336**, 565–567.
25. P. E. Batson, N. Dellby and O. L. Krivanek, Sub–angstrom resolution using aberration corrected electron optics, *Nature,* 2002, **418**, 617–620.
26. D. A. Muller, N. Nakagawa, A. Ohtomo, J. L. Grazul and H. Y. Hwang, Atomic–scale imaging of nanoengineered oxygen vacancy profiles in SrTiO3, *Nature,* 2004, **430**, 657–661.
27. X. Q. Li and W. X. Zhang, Iron nanoparticles: the core–shell structure and unique properties for Ni (II) sequestration, *Langmuir*, 2006, **22**, 4638–4642.
28. Y. P. Sun, X. Q. Li, J. S. Cao, W.-X. Zhang and H. P. Wang, Characterization of zero–valent iron nanoparticles, *Adv. Colloid Interfac.*, 2006, **120**, 47–56.

29. W. L. Yan, A. A. Herzing, X. Q. Li, C. J. Kiely and W. X. Zhang, Structural Evolution of Pd–Doped nanoscale zerovalent iron (nZVI) in aqueous media and implications for particle aging and reactivity, *Environ. Sci. Technol.,* 2010, **44**, 4288–4294.

30. Q. Wang, S. Lee and H. C. Choi, Aging Study on the Structure of Fe^0-Nanoparticles: Stabilization, Characterization, and Reactivity, *J. Phys. Chem. C*, 2010, **114***,* 2027–2033.

31. Q. Wang, S. Snyder, J. Kim and H. C. Choi, Aqueous Ethanol modified Nanoscale Zerovalent Iron in Bromate Reduction: Synthesis, Characterization, and Reactivity, *Environ. Sci. Technol.,* 2009, **43**, 3292–3299.

32. S. Kahle, Z. Deng, N. Malinowski , C. Tonnoir, A. Forment-Aliaga, N. Thontasen, G. Rinke, D. Le, V. Turkowski, T. S. Rahman, S. Rauschenbach, M. Ternes and K. Kern, The Quantum Magnetism of Individual Manganese-12-Acetate Molecular Magnets Anchored at Surfaces, *Nano Lett.*, 2012, **12**, 518−521.

33. G. Huang, X. Shi, R. A. Pinto, E. Petersen and W. J. Weber, Tunable Synthesis and Immobilization of Zero–Valent Iron Nanoparticles for Environmental Applications, *Environ. Sci. Technol.*, 2008, **42**, 8884–8889.

34. J. Lai, K. V. P. M. Shafi, A. Ulman, K. Loos, R. Popovitz–Biro, Y. Lee, T. Vogt and C. Estournes, One–Step Synthesis of Core(Cr)/Shell(γ-Fe2O3) Nanoparticles, *J. Am. Chem. Soc.*, 2005, **127**, 5730–5731.

35. C. Colliex, T. Manoubi and C. Ortiz, Electron–energy–loss–spectroscopy near–edge fine structures in the iron–oxygen system, *Phys. Rev. B*, 1991, **44**, 11402–11411.

36. N. Galvez, B. Fernandez and P. Sanchez, Comparative structural and chemical studies of ferritin cores with gradual removal of their iron contents*,* *J. Am. Chem. Soc.*, 2008, **130**, 8062–8068.

37. T. G. Sparrow, and B. G. Williams, C. N. R. Rao and J. M. Thomas, L_3/L_2 white–line intensity ratios in the electron energy–loss spectra of 3d

transition-metal oxides, *Chem. Phys. Lett.*, 1984, **108,** 547-550.

38. W. L. Yan, A. A. Herzing, X. Q. Li, C. J. Kiely and W.-X. Zhang, Nanoscale zero–valent iron (nZVI): Aspects of the core–shell structure and reactions with inorganic species in water, *J. Contam. Hydrol.*, 2010, **118**, 96–104.

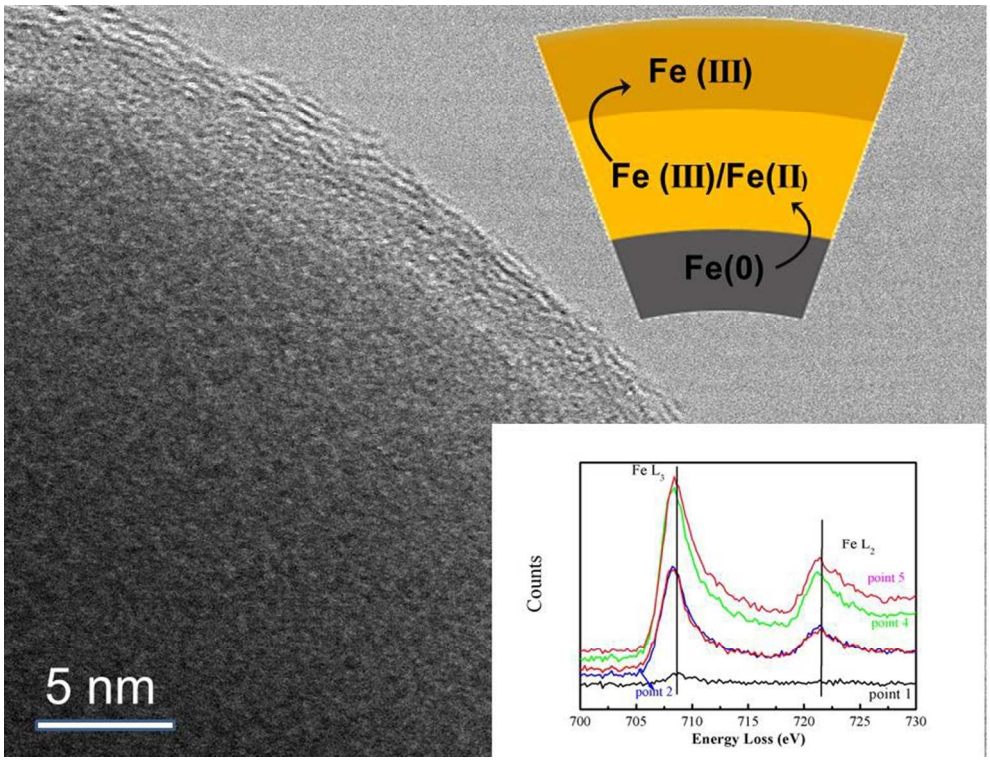

254x190mm (96 x 96 DPI)